A Study on the Role of Reaction Modeling in Multi-phase CFD-based Simulations of Chemical Looping Combustion

H. Kruggel-Emden, F. Stepanek, A. Munjiza

Oil & Gas Science and Technology – Rev. IFP Energies nouvelles, Vol. 66 (2011), No. 2, pp. 313-331

DOI: 10.2516/ogst/2010031

IFP Energies nouvelles International Conference
Rencontres Scientifiques d'IFP Energies nouvelles

Chemical Looping - An Alternative Concept for Efficient and Clean Use of Fossil Resources
La Boucle Chimique - Un concept alternatif pour un usage propre et efficace des ressources fossiles

A Study on the Role of Reaction Modeling in Multi-phase CFD-based Simulations of Chemical Looping Combustion

H. Kruggel-Emden[1,2*], F. Stepanek[1] and A. Munjiza[2]

1 Department of Chemical Engineering, South Kensington Campus, Imperial College London, SW7 2AZ, London - UK
2 Department of Engineering, Queen Mary, University of London, Mile End Road, E1 4NS, London - UK
e-mail: kruggel-emden@leat.rub.de - f.stepanek@imperial.ac.uk - a.munjiza@qmul.ac.uk
* Corresponding author

Résumé — Impact du modèle de réaction sur les simulations CFD de la combustion en boucle chimique — La combustion en boucle chimique (Chemical Looping Combustion) est une technologie de combustion efficace permettant le captage *in situ* du CO_2 pour des charges gazeuses ou solides. Dans l'optique du développement et de l'extrapolation du procédé, la CFD est un outil de simulation à fort potentiel qui s'appuie notamment sur des modèles cinétiques pour décrire les réactions gaz-solide. Ces modèles décrivant les réactions sont généralement assez simples pour limiter les temps de simulation et sont obtenus à partir d'expérimentations en thermobalance. Il y a encore peu de travaux de modélisation CFD du procédé CLC et il est difficile d'estimer l'importance du modèle décrivant les réactions chimiques sur les résultats des simulations.

Le but de ce travail est donc d'étudier la combustion de charges gazeuses H_2 et CH_4 dans des réacteurs en batch en considérant 3 matériaux transporteurs d'oxygène ($CaSO_4$, Mn_3O_4 et NiO). Quatre modèles cinétiques (le modèle à cœur rétrécissant linéaire, le modèle à cœur rétrécissant sphérique, le modèle d'Avrami-Erofeev et un modèle plus récent multi-paramètres) ont été utilisés et comparés au cas par cas.

Abstract — A Study on the Role of Reaction Modeling in Multi-phase CFD-based Simulations of Chemical Looping Combustion *— Chemical Looping Combustion is an energy efficient combustion technology for the inherent separation of carbon dioxide for both gaseous and solid fuels. For scale up and further development of this process multi-phase CFD-based simulations have a strong potential which rely on kinetic models for the solid/gaseous reactions. Reaction models are usually simple in structure in order to keep the computational cost low. They are commonly derived from thermo-gravimetric experiments. With only few CFD-based simulations performed on chemical looping combustion, there is a lack in understanding of the role and of the sensitivity of the applied chemical reaction model on the outcome of a simulation.*

The aim of this investigation is therefore the study of three different carrier materials $CaSO_4$, Mn_3O_4 and NiO with the gaseous fuels H_2 and CH_4 in a batch type reaction vessel. Four reaction models namely the linear shrinking core, the spherical shrinking core, the Avrami-Erofeev and a recently proposed multi parameter model are applied and compared on a case by case basis.

NOTATION

Variable	Unit	Denotation
A_{RZ}	(m^2)	Area of the reaction zone
a_n, a_m	(1/s)	Multi parameter model coefficients
b	(-)	Stoichiometric constant
b_n, c_n, d_m, b_m, c_m	(-)	Multi parameter model coefficients
C	(mol/m^3)	Concentration
d_p	(μm)	Particle diameter
E	(kJ/mol)	Reaction activation energy
e	(-)	Restitution coefficient
k	(m/s)	Chemical reaction rate constant
k_0	(m/s)	Chemical reaction rate factor
k'	(1/s)	Chemical reaction rate constant
k''	($m^{3n}/(mol^n \cdot s)$)	Chemical reaction rate constant
m	(-)	Exponent
n	(-)	Apparent reaction order
n, m, l	(-)	Index
p	(kPa)	Pressure
R	(kJ/(kmol·K))	Gas constant
r	($mol/(s \cdot m^3)$)	Reaction rate
r_c	(μm)	Radial position of the reaction front
r_{he}	($mol/(s \cdot m^3)$)	Heterogeneous reaction rate
r_p	(μm)	Particle radius
S	(1/μm)	Surface area
T	(K)	Temperature
t	(s)	Time
v	(m/s)	Velocity
X	(-)	Volumetric dimensionless degree of conversion
Y	(kg/kg)	Mass fraction
Z	(mol/mol)	Molar fraction

Greek letters

Variable	Unit	Denotation
ρ_g	(kg/m^3)	Gas density
ε_g	(-)	Gas volume fraction
ε_s	(-)	Solid volume fraction
ξ	(°)	Angle of internal friction

Subscripts

Variable	Denotation
0	Initial
AE	Avrami-Erofeev model
LSC	Linear shrinking core model
max	Maximal
SSC	Spherical shrinking core model
ref	Reference

INTRODUCTION

The increase in average annual surface temperature known as global warming is believed to be linked to human activity through the emissions of greenhouse gases into the earth's atmosphere [1]. As the most dominant source emissions of carbon dioxide from power generation and industrial processes can be identified. Many scientific studies come to the result that a reduction of greenhouse gas emissions in the imminent future is essential to constrain the hazardous impact of global warming [1].

A reduction of emissions could be achieved through the shift towards carbon dioxide free or neutral energy sources like biomass, nuclear, solar, water or wind energy. However, some energy sources like water power or biomass suffer from limited availability, others like wind and solar energy lack the continuous availability and nuclear power is environmentally problematic due to the still unresolved problem of long term waste handling. Therefore industrial processes and energy production have to continue to rely on fossil fuels as their main energy source in the near future.

On this background, a significant reduction in carbon dioxide emissions is feasible through methods of carbon capture and following sequestration [2, 3]. The methods available for carbon capture can be divided in three main groups as pre-combustion, oxy-fuel combustion and post-combustion technologies. Despite ongoing research most of them still result in a drop in process efficiency of 7-12% points [3, 4]. An alternative poses chemical looping combustion, which was introduced as a more energy efficient combustion approach [5, 6] based on the technical concept originally proposed by Lewis and Gilliland [7]. Ishida *et al*. [8] and Ishida and Jin [9] introduced and shaped the phrase "chemical looping combustion" for the underlying technical concept which is still used today. In chemical looping combustion a metal oxide is used to supply the necessary oxygen instead of using air. Therefore the combustion products are not diluted with nitrogen and excess oxygen, and nearly pure carbon dioxide can be sequestrated. With such an approach the efficiency drop due to carbon capture can be reduced [10, 11]. A basic outline of the process is shown in Figure 1.

The process is based on a concept with two interconnected fluidized or moving bed reactors *(Fig. 1a)* or run in non fluidized batch operation *(Fig. 1b)*. In the first case a solid oxygen carrier is circulated between both reactors and transports the necessary oxygen from the air-reactor to the fuel-reactor. Here the fuel is combusted without the presence of nitrogen. Carbon dioxide and steam are the only resulting combustion products. By condensing the water vapor, a nearly pure stream of carbon dioxide is obtained and ready for sequestration. The process can be realized through the combination of a bubbling fluidized bed operated as the fuel reactor in combination with a high velocity riser operated as air reactor as proposed by Lyngfelt *et al*. [12]. In cases where the oxidation

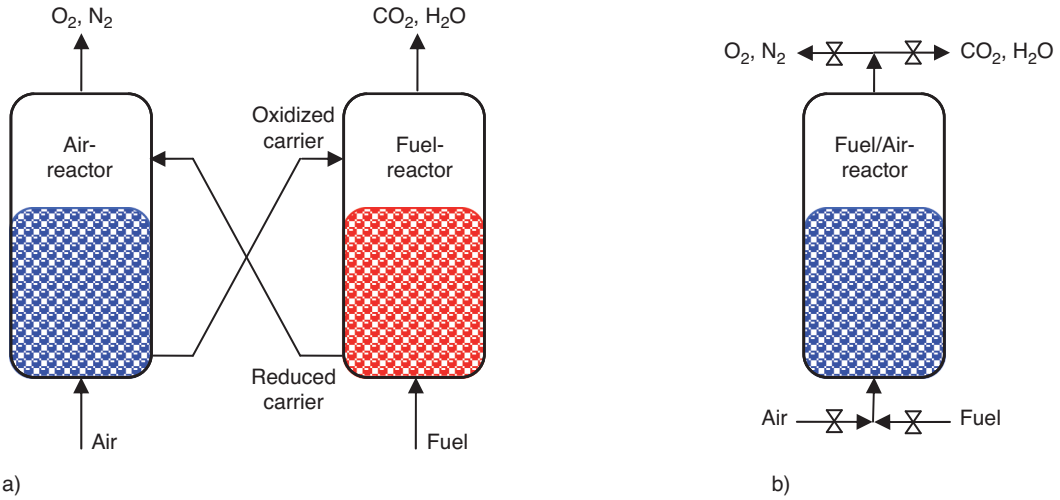

Figure 1

Possible outlines of a chemical looping combustion system: a) interconnected fluidized or moving bed system and b) a packed bed batch system with alternating flow.

reaction in the air reactor is not sufficiently fast a concept involving a double combination of riser and bubbling fluidized bed can be applied as proposed by Son and Kim [13] or moving beds as proposed by Gnanapragasam *et al*. [14] or Fan *et al*. [15] can be inherited. Alternatively a batch operation of the chemical looping combustion process is possible as suggested by Noorman *et al*. [16, 17]. In this case the vessel filled with the oxygen carrier is alternately used as air- and fuel-reactor using a high temperature gas switching system. In order to get a continuous stream of hot gas feedable to a gas turbine at least two reactors have to be operated in parallel. The packed bed concept has the advantage of avoiding any particle/gas separation through a cyclone and is gentler to the particles. However it can not be operated with solid fuels and the design and operation of the hot gas switching system is problematic [16].

For all chemical looping combustion processes suitable oxygen carrier materials have to be provided. Suitable materials should have a high oxidation and reduction activity, remain stable under repeated oxidations/reductions, possess enough mechanical strength, be resilient to agglomeration, be environmental friendly and be of low cost. As materials metal oxides as cobalt, copper, iron, manganese and nickel are deployed. However, materials used for flue gas desulphurization such as calcium sulfide are also applicable [18, 19]. Very often the active metal oxide is supported by an inert carrier material to improve mechanical strength. A comprehensive overview of the important aspects related to the choice and use of certain oxygen carriers can be found in the recent review by Hossaina and de Lasa [20].

With successful operation of laboratory scale chemical looping combustion systems by several research groups with different carrier materials and fuels up to 140 kW_{th} [21-26] and the aim to realize even larger systems up to 1 MW_{th} [27, 28, 19] the demand for applicable modeling strategies in case of chemical looping combustion systems grows. Modeling strategies are essential for the elementary design of chemical looping systems, the sensitivity study of parameters and the scale up of equipment for the use within industrial size processes.

In the following a review of different modeling strategies with special focus on the applied kinetic models is performed. The review of simulations reveals that reaction kinetics is often implemented vaguely especially in case of fluidized systems modeled through the multi-phase CFD-approach. The aim of this study is therefore to investigate the effect of the application of different kinetic models on macroscopic results of typically operated batch fluidized systems. The review of simulation approaches is followed by an outline of the applied simulation framework, an overview over simulation parameters and the simulation results.

1 MODELING OF CHEMICAL LOOPING COMBUSTION: CURRENT STATE OF RESEARCH

In general modeling of chemical looping processes can be achieved on different levels of accuracy with very differing computational costs and varying significance of calculated results. It can be distinguished between particle based methods, multi-phase CFD-models and macroscopic continuum approaches. In the given order their computational demand is decreasing.

1.1 Particle Based Methods

For chemical looping combustion no particle based methods have been applied, however, their potential use for reacting particle systems has been outlined in studies on combustion processes in slow moving dense beds by *e.g.* Simsek *et al.* [29]. Particle based methods like the discrete element approach allow to model each particle in the system individually representing its temperature, composition, position and velocity. To model the gaseous phase classical CFD-models can be applied which need to be coupled with a discrete phase model [30]. The overall system behavior is given by the interaction of all individual particles along with the surrounding gas phase. Despite their high level of accuracy their applicability is limited to systems of up to 10^6 particles even on modern computer systems. This number is often already exceeded for smaller laboratory scale fluidized beds [20].

1.2 Multi-phase Fluid Dynamics

The limitation of considerable particle numbers can be overcome through models based on multi-phase fluid dynamics. These models assume the particle and fluid phase to be modeled in the framework of the Navier-Stokes equations using averaged quantities. Closure equations for the solid phase pressure and the solid phase viscosity have to be provided derived from the kinetic theory of granular flow [31]. The kinetic theory of granular flow is an extension of the classical kinetic gas theory realizing for inelastic particle/particle interaction [32, 33]. Although these models have been frequently used for bubbling fluidized beds [34], mixing [35], downflow reactors [36] and spouted beds [37], Jung and Gamwo [38] were the first to apply multi-phase CFD modeling for chemical looping combustion processes. In their study the combustion of methane with NiO as an oxygen carrier was considered. Reduction and oxidation of the carrier are described by the two reactions:

$$4NiO + CH_4 \rightarrow CO_2 + 2H_2O + 4Ni \quad (1)$$

$$4Ni + 2O_2 \rightarrow 4NiO \quad (2)$$

Jung and Gamwo [38] considered only the oxidation of methane occurring in the fuel reactor which is operated as a bubbling fluidized bed. For the kinetic modeling of this reaction they relied on an shrinking core model as proposed by Ryu *et al.* [39] which is written in integral form as:

$$t = \frac{C_{NiO0} r_p}{bkC_{CH_4 0}} [1 - (1 - X)^{1/3}] \quad (3)$$

with the stoichiometric coefficient $b = 4$, C_{NiO0} the initial concentration of the solid oxygen carrier material, $C_{CH_4 0}$ the bulk concentration of the gaseous reactant, $r_p = 80$ µm the initial particle radius and X the volumetric dimensionless degree of conversion. The chemical reaction rate constant k given in (m/s) was derived by Ryu *et al.* [39] through thermal gravimetrical analysis technique as:

$$k = k_0 \exp\left(\frac{E}{RT}\right) \quad (4)$$

with $E = 37\,070$ kJ/(kmol) and $k_0 = 3.27 \cdot 10^{-2}$ m/s.

In their paper Ryu *et al.* [39] provide an equation to calculate C_{NiO0}, however, not all necessary data like densities and molar weights are provided rendering it impossible to calculate this value directly. Experiments were performed at three temperatures $T = 1\,023$ K, $T = 973$ K and $T = 873$K at a volume fraction of CH_4 of 0.0504 m^3/m^3 at atmospheric pressure. Based on a best fit for C_{NiO0} derived as 2 701 mol/m^3 Figure 2 reveals a discrepancy between the calculated degree of conversion of NiO for the shrinking core model based in Equations (3, 4) (solid line) and graphical results (dashed line) published in the original paper [39].

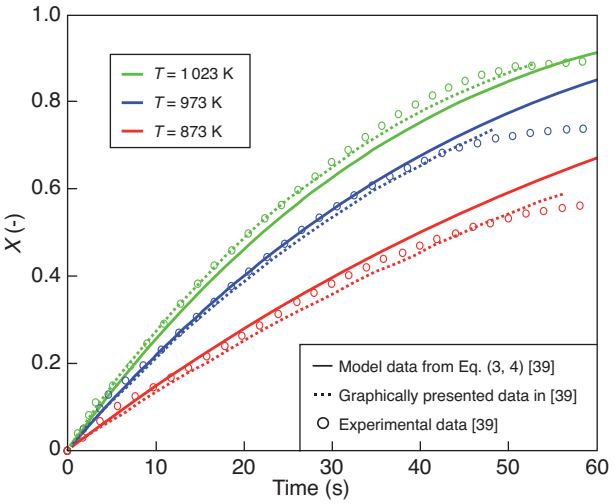

Figure 2

Discrepancy in modeled data given by Ryu *et al.* [39] for the conversion of NiO particles calculated through Equations (3, 4) and as graphically stated in the original paper in regard to their experimental results.

It is noticeable that conversion is represented too low at high temperatures and exaggerated for low temperatures based in Equations (3, 4) and not as good as stated by Ryu *et al.* [39]. The kinetic data from Equation (4) is used in the CFD-based study of Jung and Gamwo [38].

To calculate the reaction rate, Jung and Gamwo use an equation as given below where S_0 is the surface area with:

$$r = -kS_0\varepsilon_g \frac{\rho_g Y_{CH_4}}{M_{CH_4}} = -kS_0\varepsilon_g C_{CH_4} \quad (5)$$

$$S_0 = \frac{6}{d_p}\varepsilon_S Y_{O_2} \tag{6}$$

The given equation for the reaction rate is linearly dependent on the gas fraction ε_g. The surface area S_0 is also linearly dependent on the mass fraction of oxygen Y_{O_2} which is the bonded oxygen within the NiO. The bonded oxygen is a measure for the degree of conversion of the carrier material. Other authors like Levenspiel [40] or Syamlal [41] define the rate of reaction differently. Firstly they keep r independent of ε_g:

$$r = -kS_0 \frac{\rho_g Y_{CH_4}}{M_{CH_4}} = -kS_0 C_{CH_4} \tag{7}$$

Secondly due to the fact that an unreacted shrinking core model is used S_0 is dependent on the degree of conversion X through a nonlinear relation with:

$$S_0 = \frac{6}{d_p}\varepsilon_S (1-X)^{2/3} \tag{8}$$

where X is the volumetric dimensionless degree of conversion. The degree of conversion X is on the one hand linked with the ratio between the radial position of the reaction front within the particle r_c and the particle radius r_p and on the other hand with the mass fractions Y of Ni and NiO through:

$$(1-X)^{1/3} = r_c/r_p = (Y_{Ni}/\rho_{Ni})/(Y_{Ni}/\rho_{Ni} + Y_{NiO}/\rho_{NiO}) \tag{9}$$

The differences in modeling with both approaches, the sets of Equations (5, 6) and (7-9) are outlined in Figure 3. Following the assumption of the unreacted shrinking core model experimentally expected reaction rates (circles) are scaled by 2/3 due to the fact, that Jung and Gamwo use particles of r_p = 120 µm instead of r_p = 80 µm as used by Ryu *et al*. [39]. Reaction rates calculated from Equations (5, 6) are shown as dashed lines, rates calculated from Equations (7-9) are plotted as solid lines.

For comparison two different gas fractions are considered with ε_g = 0.4 in Figure 3a and ε_g = 0.8 in Figure 3b. Experimentally derived reaction rates for both cases differ due to different values calculated for S_0. The model based in Equations (5, 6) underpredicts the reaction rates strongly for low gas fractions. In case of larger gas fractions the deviation between both models tends to become smaller. Due to the linear dependency of the reaction rate on the conversion the model by Jung and Gamwo [38] produces significantly different results compared to nonlinear models following Levenspiel [40] or Syamlal [41].

A further example of multi-phase CFD modelling applied to chemical looping combustion processes is given by Deng *et al*. [42, 43] and Jin *et al*. [44]. The authors were interested in the capabilities of CaS as an oxygen carrier material. The reduction and oxidation of the carrier material are given by the two reactions:

$$CaSO_4 + 4H_2 \rightarrow CaS + 4H_2O \tag{10}$$

$$CaS + 2O_2 \rightarrow CaSO_4 \tag{11}$$

Deng, Jin and coworkers are only interested in the fuel reactor reaction (10). For the modeling of the kinetics they rely on data by Kim and Sohn [18]. Kim and Sohn suggest the use of the Avrami-Erofeev nucleation growth model with:

$$t = 1/k' \cdot (-\ln(1-X))^{1/m} \tag{12}$$

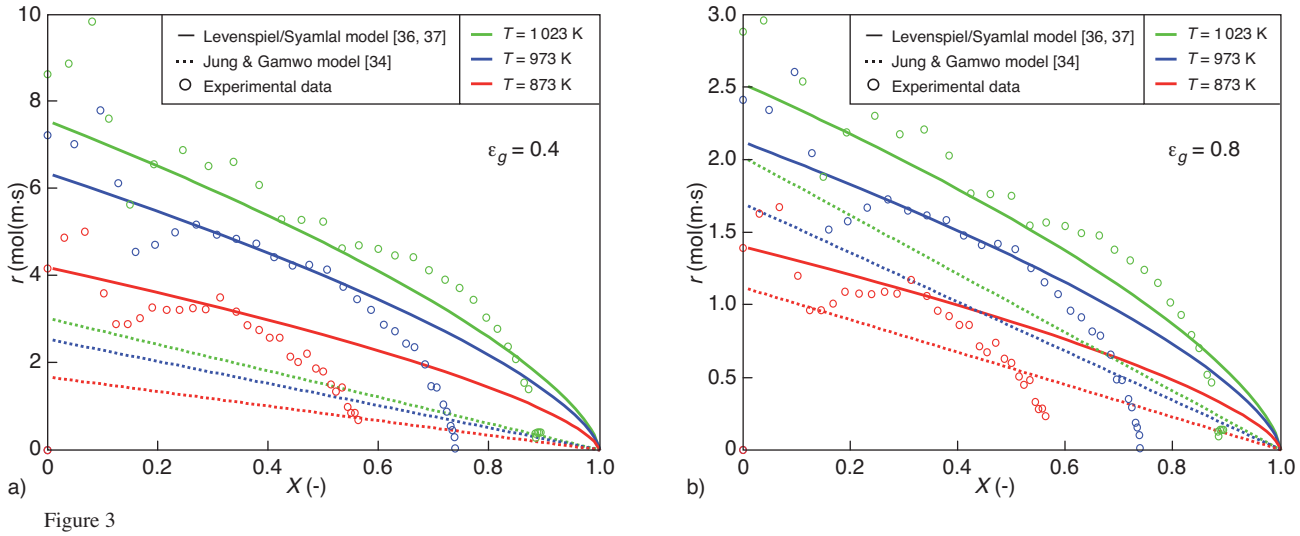

Figure 3

Reaction rate as obtained from literature from Ryu *et al*. [39] scaled by particle size and calculated from Equations (5, 6) following Jung and Gamwo [38] and motivated by Equations (7-9) as suggested by Levenspiel [40] and Syamlal *et al*. [41]: a) ε_g = 0.4 and b) ε_g = 0.8.

where the kinetic reaction constant k' in (1/s) is given as:

$$k' = k_1 \cdot p_{H_2} \cdot e^{-\frac{E}{R \cdot T}} \quad (13)$$

where $R = 8.314472$ J/mol·K^{-1} is the gas constant, $E = 151$kJ/kmol the activation energy, $k_1 = 70.83 \cdot 1/(s \cdot kPa)$ and $m = 1.16$ with T given in (K) and p in (kPa). Deng and coworkers, however, do not use an Avrami-Erofeev model but apply its kinetic constant to a linear shrinking core model written as:

$$t = X/k' \quad (14)$$

Figure 4 reveals the effects of applying the kinetic constant from the Avrami-Erofeev model to a linear model without any adjustment. In general a linear model (dashed line) is only to a very limited extent able to represent the experimental conversion data of $CaSO_4$ derived for varying H_2 concentrations and different temperatures. In contrast the Avrami-Erofeev model (solid line) is quite capable of doing this. Far more striking is the fact that the slopes and thereby the reaction rates at large gas concentrations and high temperatures are strongly overpredicted through the use of the kinetic constants within a linear model.

1.3 Macroscopic Continuum Models

In contrast to the previous approaches macroscopic continuum models which are the least accurate, but the most computational efficient methods are based on separating the computational domain in the different reaction vessels into different zones which are further simplifications of the cell structure used in

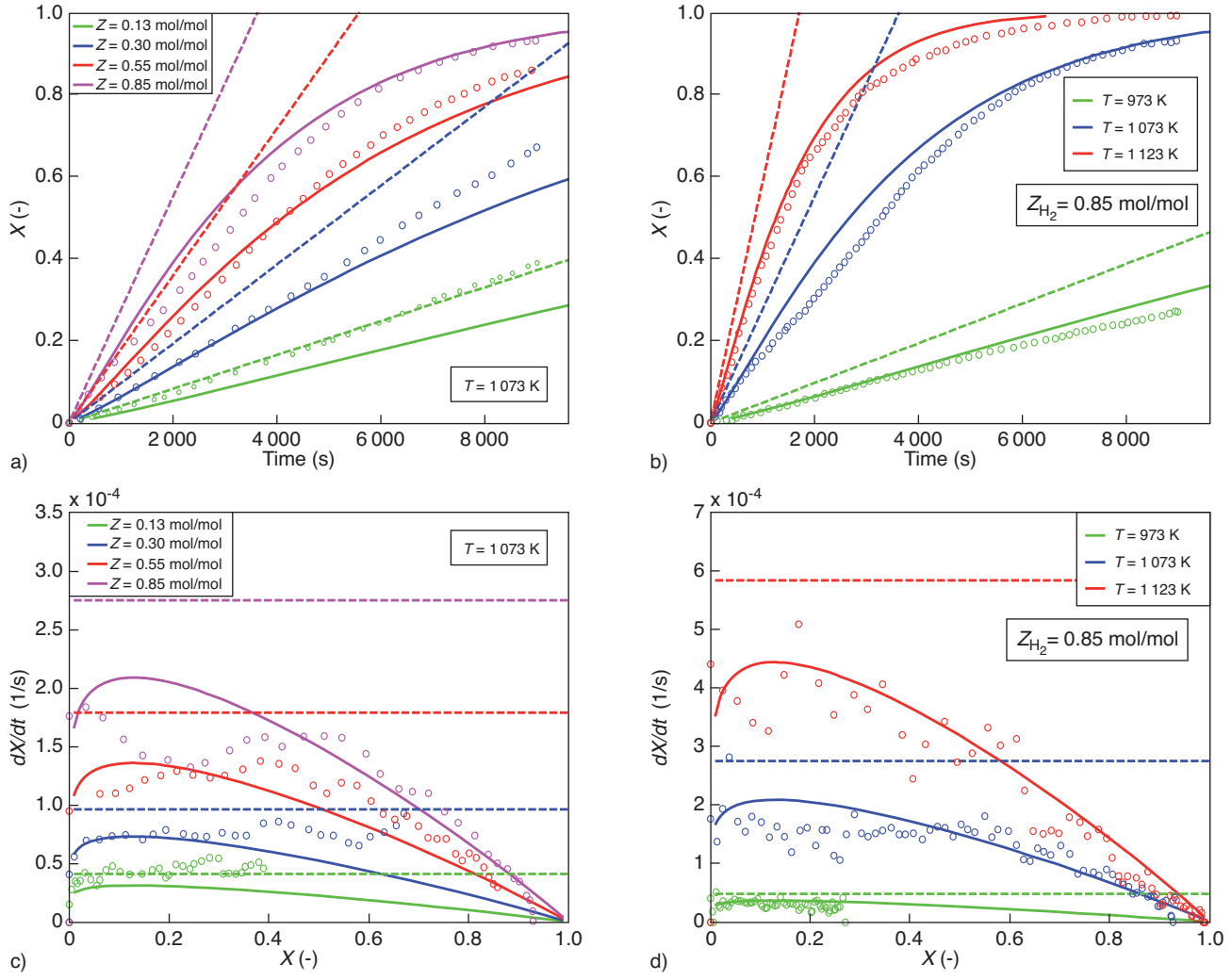

Figure 4

Degree of conversion (a, c) and conversion rate (b, d) for $CaSO_4$ as modeled and experimentally obtained from Kim and Sohn [18] and as modeled by Deng *et al.* [42, 43] with gas temperature T and molar fraction Z of the gaseous reactant: (---) model used by Deng *et al.*, (—) Avrami-Erofeev model and experimental data (○) derived from Kim and Sohn.

the multi-phase CFD approaches. Formation of internal structures within the domain like bubbles or the development of gradients within one zone is often not resolved. However, the interaction of vessels through the circulation of carrier material can be considered in a transient way. These models found application by Xu *et al*. [45], Bolhar-Nordenkampf [46] or Kolbitsch [47] for fluidized systems and by Noorman *et al*. [16] for packed beds.

2 APPLIED SIMULATION FRAMEWORK

As the mathematical model framework in the study here a two-phase CFD approach is applied consisting of a gaseous and a particle phase. Balance equations are solved for each individual phase regarding the exchange of momentum, heat and mass transfer. The solid phase is modeled based on the kinetic theory of granular flow. As framework the commercial CFD-software Fluent 6.3.16 is used. Details on the underlying equations can be found in [38, 48, 49].

2.1 Modeling of the Reaction Kinetics

For chemical looping combustion mainly two types of models are widely applied for both the oxidation and the reduction of the carrier material: Shrinking core models and nucleation growth models. The shrinking core models can be further divided into different groups depending on their governing mechanisms and the involved geometrical shape of the carrier. For further details see Hossaina and de Lasa [20] and Levenspiel [40]. Already introduced in the previous sections are the reaction based spherical shrinking core approach through Equation (3), the reaction based linear shrinking core approach through Equation (14) and the nucleation growth model through Equation (12).

The conversion rates for the spherical and linear shrinking core approach and the nucleation growth model can be calculated as:

$$dX/dt_{SSC} = 3 \cdot b \cdot k'' \cdot \exp\left(-\frac{E}{R \cdot T}\right) \cdot C_{gas}^{n} (1-X)^{2/3} \tag{15}$$

$$dX/dt_{LSC} = b \cdot k'' \cdot \exp\left(-\frac{E}{R \cdot T}\right) \cdot C_{gas}^{n} \tag{16}$$

$$dX/dt_{AE} = -m \cdot 1/b \cdot k'' \cdot C_{gas}^{n} \cdot \exp\left(-\frac{E}{R \cdot T}\right) \cdot (X-1)(-\ln(1-X))^{\left(\frac{m-1}{m}\right)} \tag{17}$$

with the stoichiometric coefficient of the solid reactant b and C_{gas} the bulk concentration of the gaseous reactant.

In addition to these models Kruggel-Emden *et al*. [50] recently suggested the application of empirical polynomial based models for the representation of the reaction rate. These models are enabling a more accurate representation of the dependency of the reaction rate on the degree of conversion especially considering the fact that not always a full conversion of the carrier material is possible:

$$dX/dt_{MP} = \sum_{n=1}^{l} a_n \left(X/X_{ref}\right)^{b_n} \left(Y_{gas}/Y_{gasref}\right)^{c_n} \left(T/T_{ref}\right)^{d_n} + \sum_{m=1+l}^{2l} a_m \left(Y_{gas}/Y_{gasref}\right)^{b_m} \left(T/T_{ref}\right)^{c_m} \tag{18}$$

Here a_n, b_n, c_n, d_n, a_m, b_m, c_m are empirical coefficients, Y_{gas} is the bulk mass fraction of the gaseous reactant and T_{ref}, X_{ref}, Y_{gasref} reference values to make T/T_{ref}, X/X_{ref}, Y_{gas}/Y_{gasref} dimensionless. For all applied models the heterogeneous reaction rate is important for the determination of the mass transfer between both solid and fluid phase and for the species transport equation given as:

$$r_{he} = 1/b \cdot dX/dt \cdot C_{Me0} \tag{19}$$

2.2 Simulation Parameters

The set of partial differential equations for the two-phase framework are solved through the finite volume method. The pressure-velocity coupling for both fluid and solid phase is realized through the phase coupled SIMPLE algorithm. The second-order-upwind-method was employed. A schematic of the fluidized bed is outlined in Figure 5.

The gas inlet is defined through a uniform velocity inlet. The gas leaves the vessel through an outlet at the top of the vessel. The domain was discretized through 2 500 rectangular cells in 2D. Grid refinement was tested and has only minor effect on the flow behavior. A time step of 0.0001 s was

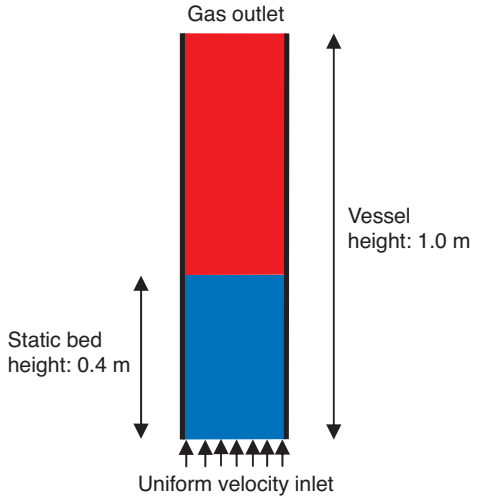

Figure 5
Schematic of the investigated fluidized bed.

selected to ensure a convergence criterion of 10^{-3} for all quantities. The standard *k*-ε model was used for both fluid and solid phase with a standard wall function to model for turbulence. For details on the use of a *k*-ε model within a two-phase framework see Gryczka *et al*. [37]. Fluid particle momentum exchange was model through the approach by Gidaspow and heat transfer by the model of Gunn as outlined in [48]. The general simulation parameters are stated in Table 1.

Three different materials $CaSO_4$, Mn_3O_4 and NiO were selected as carrier. Deliberately $CaSO_4$ was chosen as applied in the studies by Deng *et al*. [42, 43] and NiO as used by Jung and Gamwo [38]. The simulation conditions are selected similar to those by Deng *et al*. [42, 43]. An outline of the material sensitive simulation parameters is given in Table 2. The parameters used for the adjustment of the kinetic models (15-18) are given in Kruggel-Emden *et al*. [50].

TABLE 1

General system properties and parameters for the simulations

Width of vessel (m)	0.25
Height of vessel (m)	1.0
Initial bed height (m)	0.4
Initial solids packing (-)	0.48
Angle of internal friction ξ (°)	30
Maximal packing limit $\varepsilon_{s,max}$ (-)	0.6
Restitution coefficient e (-)	0.9
Grid number (-)	2 500
Grid size (m)	0.01 × 0.01
Time interval (s)	0.0001

TABLE 2

Oxygen carrier material sensitive simulation parameters

Reduction of $CaSO_4$	
Governing reaction	$CaSO_4 + 4H_2 \rightarrow CaS + 4H_2O$
Inlet gas velocity (m/s)	0.32; 0.9
Inlet gas composition (%)	H_2: 100; H_2O: 0
Initial solid phase composition (%)	$CaSO_4$: 100; CaS: 0
Particle diameter (mm)	0.275
Initial solid temperature (K)	1 123
Inlet gas temperature (K)	1 123
Reduction of Mn_3O_4	
Governing reaction	$4Mn_3O_4 + CH_4 \rightarrow 12MnO + CO_2 + 2H_2O$
Inlet gas velocity (m/s)	0.3
Inlet gas composition for $t < 1$ s (%)	CH_4: 0; H_2O: 0; CO_2: 100
Inlet gas composition for $t > 1$ s (%)	CH_4: 8.352 ; H_2O: 0; CO_2: 91.648
Initial solid phase composition for $X = 0$ (%)	ZrO_2: 59.98; Mn_3O_4: 39.99; MnO: 0; Air: 0.03
Initial solid phase composition for $X = 0.8$ (%)	ZrO_2: 57.4; Mn_3O_4: 7.65; MnO: 34.9; Air: 0.03
Particle diameter (mm)	0.1525
Initial solid temperature (K)	1 223
Inlet gas temperature (K)	1 223
Reduction of NiO	
Governing reaction	$4NiO + CH_4 \rightarrow CO_2 + 2H_2O + 4Ni$
Inlet gas velocity (m/s)	0.3
Inlet gas composition for $t < 1$ s (%)	CH_4: 0; H_2O: 0; CO_2: 100
Inlet gas composition for $t > 1$ s (%)	CH_4: 8.352 ; H_2O: 0; CO_2: 91.648
Initial solid phase composition for $X = 0$ (%)	$MgAl_2O_4$: 59.99; NiO: 39.99; Ni: 0; Air: 0.02
Initial solid phase composition for $X = 0.8$ (%)	$MgAl_2O_4$: 54.17; NiO: 7.22; Ni: 38.6; Air: 0.01
Particle diameter (mm)	0.1525
Initial solid temperature (K)	1 223
Inlet gas temperature (K)	1 223

3 COMPUTATIONAL RESULTS AND DISCUSSION

3.1 Reduction of the Carrier Material $CaSO_4$

As a first test case $CaSO_4$ was fluidized in a reactor with gas velocities of $v = 0.32$ m/s and $v = 0.9$ m/s. A gas velocity of $v = 0.32$ m/s was initially proposed by Deng *et al*. [43] which is however very close to the fluidization limit. Therefore a larger velocity of $v = 0.9$ m/s was also considered lying in the slugging regime guaranteeing for a stronger dynamics within the vessel. Figure 6 outlines data on the conversion speed of $CaSO_4$ derived from experimental results by Kim and Sohn [18]. The four different reaction models introduced in Section 2.1 were adjusted to the experimental data. Details can be found in Kruggel-Emden *et al*. [50]. Results indicate that all three the Avrami-Erofeev, the spherical shrinking core and the multi parameter model are quite capable of modeling the reaction kinetics over wide ranges of conversion. It is, however, difficult to pinpoint the best model among these three. Particularly at very low degrees of conversion the experimental data favors the nucleation growth model at certain temperature levels and gas concentrations, which leads to a zero conversion rate at zero conversion in the model. However, at other temperatures and concentrations this conclusion can not be drawn. It is obvious from the progression of the conversion speed that the use of a linear shrinking core model is not suitable over wider conversion ranges.

Results for the mass fraction of H_2 and mass fraction H_2O both considered at the outlet of the vessel and the mass fraction of CaS in the solid phase are plotted over time in Figure 7. Figures (7a, c, e) are thereby related to the lower velocity of $v = 0.32$ m/s and Figures (7b, d, f) related to the velocity of $v = 0.9$ m/s. Keeping in mind the slow reactivity of $CaSO_4$, the time scales of just up to 10 s relate to only incrementally reacted $CaSO_4$ and therefore a marginal degree of conversion X. As obvious from Figure 6 a low conversion results in significant differences between the reaction models for the reaction rate.

The fastest rates are reported by the spherical shrinking core model and the multi parameter model, followed by the linear shrinking core model adjusted to match a good overall reaction rate. The Avrami-Erofeev model results in low reaction rates at low degrees of conversion. With no full conversion of the fuel gas H_2 achieved within the fluidized bed, results for the mass fractions of H_2 and H_2O at the outlet vary strongly being a result of the varying reaction rates predicted by Figure 6. Although there are differences in the reaction rates for the multi parameter model and the spherical shrinking core approach, those do not get obvious from Figure 7 for the low gas velocity, but to some extend for the larger velocity. The oscillations in the outlet gas concentrations at the larger fluidization velocity are a result of the stronger dynamics within the fluidized bed due to stronger bubble formation

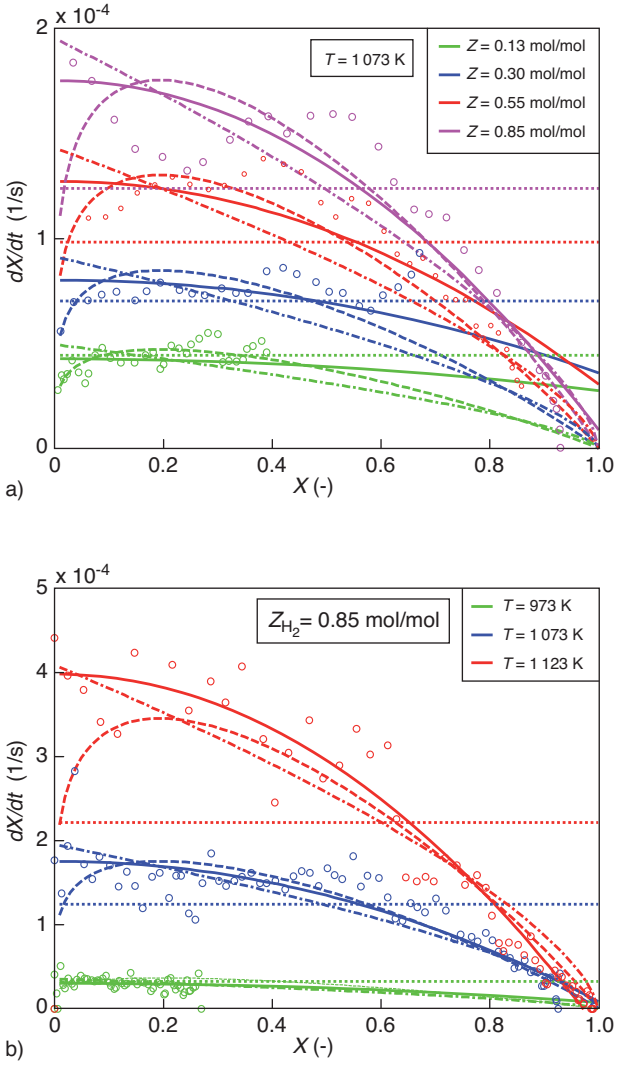

Figure 6

Conversion speed of $CaSO_4$ with H_2 at the gas temperature T and molar fraction Z of H_2: (- · -) spherical shrinking core model, (···) linear shrinking core model, (---) Avrami-Erofeev model, (—) multi parameter model, (○) experimental data derived by Kim and Sohn [18].

and slugging. Due to the fact of an incomplete conversion of the fuel gas different reaction models lead to differences in the amount of CaS formed within the fluidized bed and therefore of course in the progression of the overall conversion. Under the chosen operation conditions which were selected in accordance with Deng *et al*. [43] for the small fluidization velocity it is obvious that the times till full conversion of the solid phase vary strongly for the four investigated kinetic models.

Figure 8 shows a snapshot of the fuel gas concentration of H_2 within the fluidized bed at $t = 10$ s for the two different fluidization velocities applied. Whereas at the low velocity a

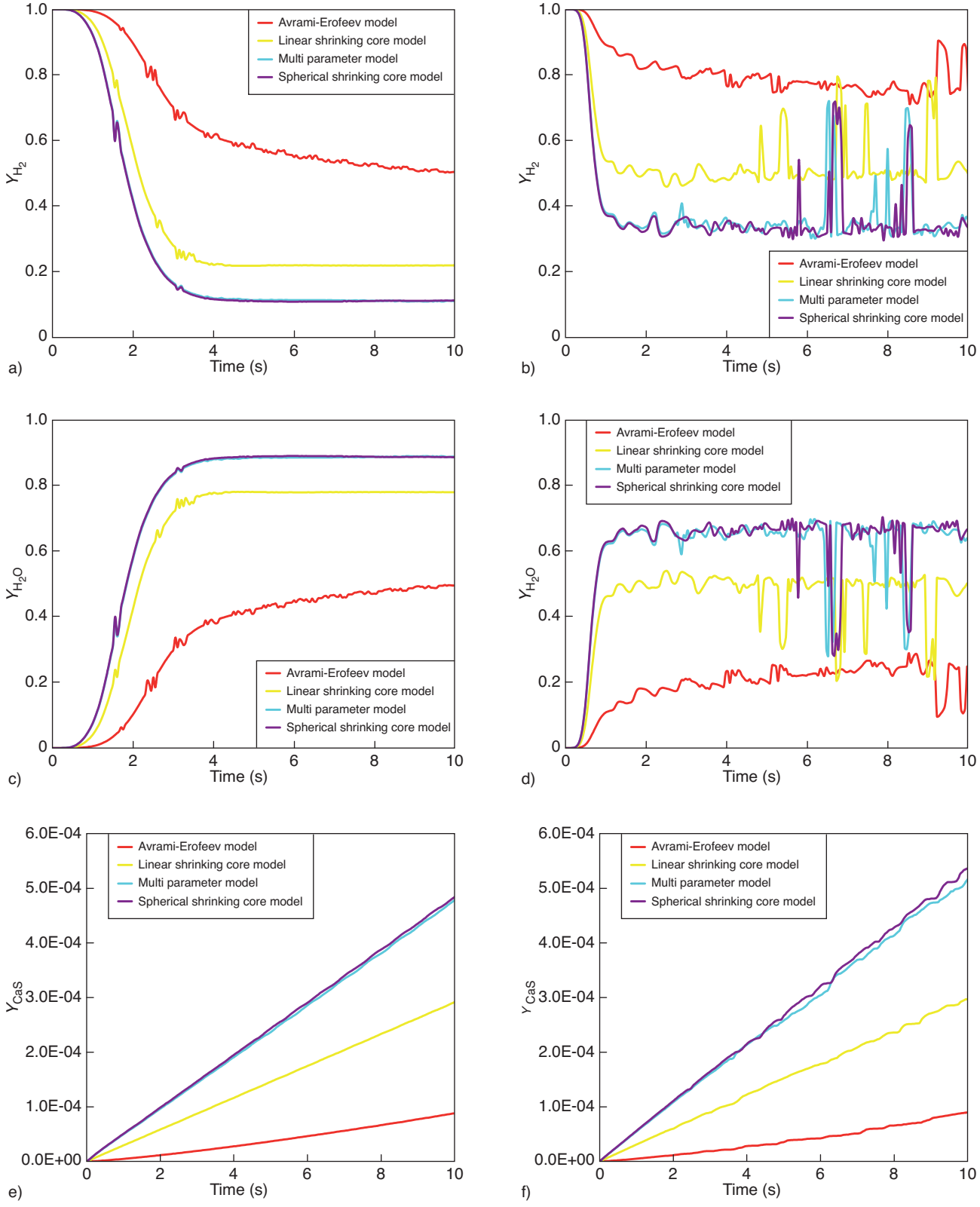

Figure 7

Mass fraction of H_2 (a, b) and mass fraction H_2O (c, d) at the outlet of the vessel and mass fraction of CaS (e, f) in the solid phase over time. Fuel inlet velocity: (a, c, e) $v = 0.32$ m/s and (b, d, f) $v = 0.9$ m/s.

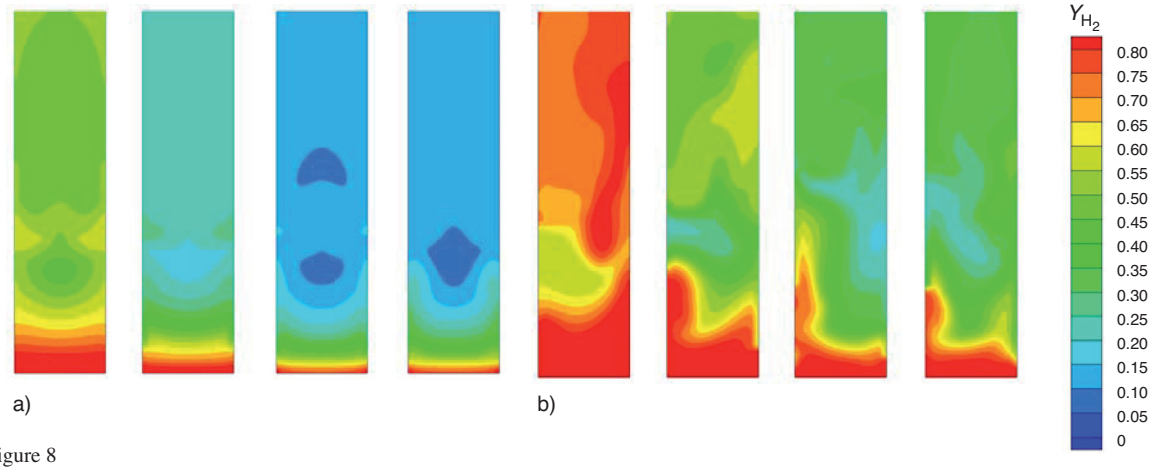

Figure 8

Mass fraction of H_2 within the fluidized bed at $t = 10$ s: a) $v = 0.32$ m/s, b) $v = 0.9$ m/s. Reaction models from left to right: Avrami-Erofeev model, linear shrinking core model, multi parameter model and spherical shrinking core model.

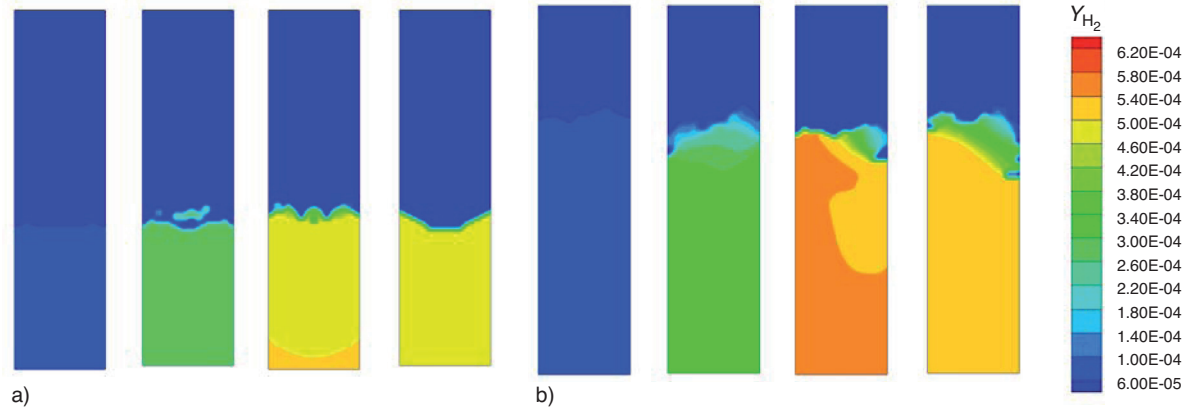

Figure 9

Mass fraction of CaS within the fluidized bed at $t = 10$ s: a) $v = 0.32$ m/s, b) $v = 0.9$ m/s. Reaction models from left to right: Avrami-Erofeev model, linear shrinking core model, multi parameter model and spherical shrinking core model.

clear lamellar reaction zone can be identified it gets frayed at the larger velocity. Different reaction models lead to differently large reaction zones.

In Figure 9, a snapshot of the concentration of CaS within the vessel at $t = 10$ s is displayed. The distribution of the different concentrations of CaS within the solid phase is very homogenous outlining a strong mixing within the solid phase. Already after the short simulation time of $t = 10$ s applied different models lead to significant different concentrations of CaS within the solid phase of the fluidized bed.

3.2 Reduction of the Carrier Material Mn_3O_4

As a second carrier material Mn_3O_4 was investigated which has a much higher reactivity than $CaSO_4$ but has a low oxygen carrier capacity compared to other metal carrier materials [20]. A fluidization velocity of $v = 0.3$ m/s was selected. The behavior of Mn_3O_4 is firstly investigated for the fully unreacted carrier material of $X_0 = 0$ and later for a partly reacted material of $X_0 = 0.8$. In Figure 10, the speed of conversion of Mn_3O_4 over the degree of conversion is plotted. Similar to $CaSO_4$ all three models as the Avrami-Erofeev, the spherical shrinking core and the multi parameter model give a fairly good representation of the experimental data derived from experiments by Zafar *et al*. [51] and Johansson *et al*. [52]. From the data a clear nucleation growth mechanism with a zero conversion rate at zero degree of conversion is not detectable. Additionally at low degrees of conversion the spherical shrinking core model leads to overstated reaction rates. Therefore best modeling of the kinetic data is achieved through the multi parameter model. The linear shrinking core model can be applied over narrow ranges of conversion but

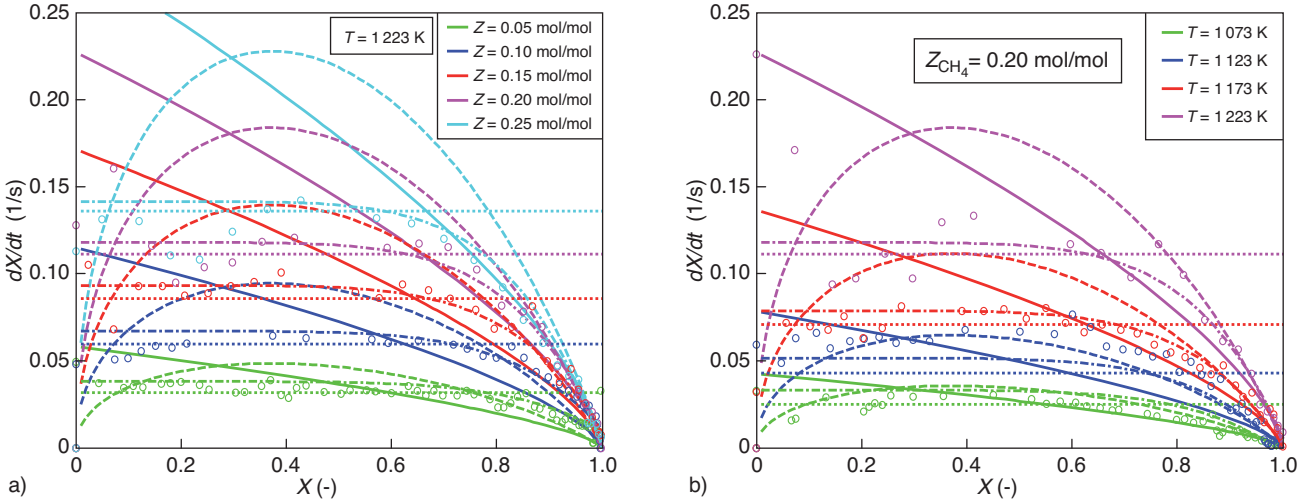

Figure 10

Conversion speed of Mn_3O_4 particles with CH_4 at the gas temperature T and molar fraction Z of CH_4: (—) spherical shrinking core model, (···) linear shrinking core model, (---) Avrami-Erofeev model, (-·-) multi parameter model, (○) experimental data derived by Zafar *et al*. [51] and Johansson *et al*. [52].

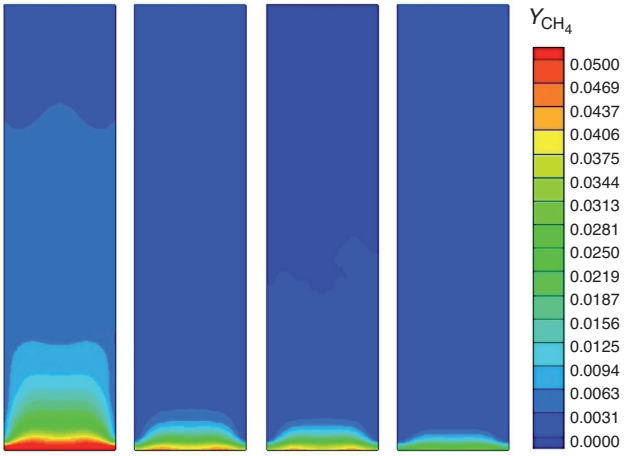

Figure 11

Mass fraction of CH_4 within the fluidized bed at t = 2 s. Reaction models from left to right: Avrami-Erofeev model, linear shrinking core model, multi parameter model and spherical shrinking core model.

fails when applied over larger intervals reporting a misleading constant conversion rate there.

Figure 11 gives a snapshot of the concentration of methane within the fluidized bed at t = 2 s. The reaction of methane within the simulated bed setup is nearly complete. Despite the different reaction rates reported from different reaction models the outlet gas contains nearly no CH_4 for all models. Different reactions models however result in differently pronounced reaction zones.

Results for the fully unreacted Mn_3O_4 are plotted in Figure 12. If the size of the reaction zone is defined as the area within the vessel's solid phase where the CH_4 concentration is above a certain threshold selected as $Y > 0.01$, than the size of the reaction zone can be calculated and plotted over time as shown in Figure 12a. The Avrami-Erofeev model results in a large reaction zone at low degrees of conversion which is declining over time. Eventually it becomes smaller than the sizes reported for the linear and the multi parameter model. The spherical shrinking core model leads to the smallest reaction zone corresponding to the fastest reaction rates. These results are in correspondence with prediction of the reaction rate over the degree of conversion displayed in Figure 10. Due to the fact that the conversion of methane within the fuel reactor is complete, the models reveal no differences in the mass fraction of MnO reported in the vessel over time as plotted in Figure 12b. Furthermore, both the average temperature within the solid phase and the gas outlet temperature which are declining over time due to the endothermic nature of the reaction, reveal no deviations as shown in Figures 12c and 12d.

In case of a advanced degree of conversion (X_0 = 0.8) of the Mn_3O_4 results for the previously considered properties are significantly differing for the four reaction models. Figure 13a reveals insight into the size of the reaction zone over time assuming a limit of $Y > 0.01$. From $X_0 = 0.8$ onwards the reaction rates are developing significantly different from each other *(Fig. 10)*. In addition the content of Mn_3O_4 in the solid phase is dropping reducing the amount of oxygen that could be released. Both affects superpose and lead to a growing reaction zone. The Avrami-Erofeev model results in the

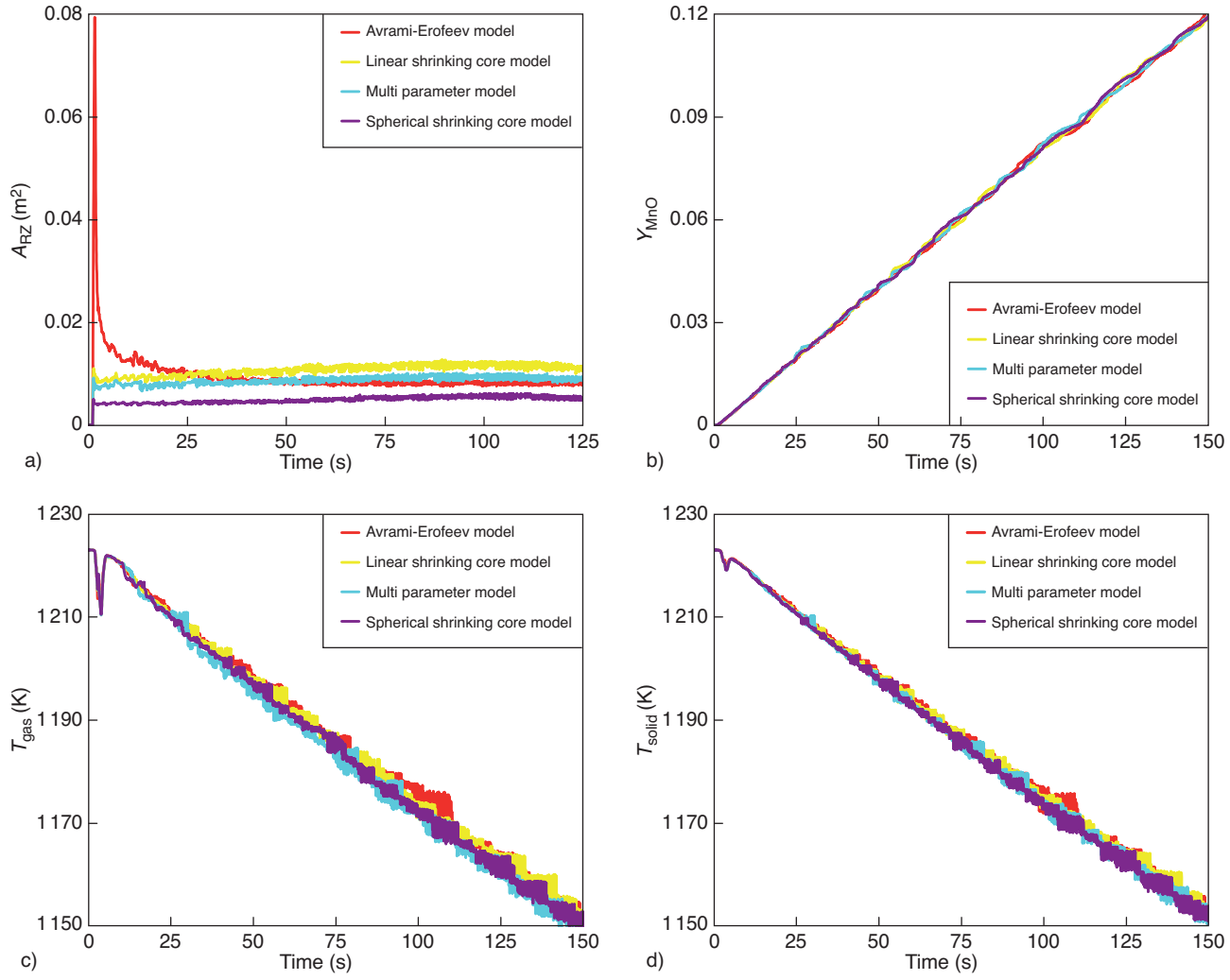

Figure 12

a) Area of the reaction zone, b) mass fraction of MnO in the solid phase, c) gas temperature at the outlet and d) temperature of the solid phase over time for $X_0 = 0$.

largest size increase of the reaction zone followed by the multi parameter model and the linear and spherical shrinking core model. The limiting value of $A_{RZ} = 0.16$ m^2 is a consequence of the maximal extension of the dense bed region when fluidized. Figure 13b gives insight into the MnO content of the solid phase. Starting with the same MnO content at $t = 0$ s the application of the different reaction models results in a varying MnO content of the solid phase over time. Figure 13c gives insight into the solid temperature. Due to the endothermic nature of the reaction the solid bed temperature is dropping over time. Due to the fact that the formation of MnO is different for the considered models the evolution of the solid temperature is also affected. It can be seen that after a certain time the solid temperature is rising again due to the fact, that the fluidizing methane/carbon dioxide mixture releases its heat which is not consumed through the earlier ongoing reaction. Figure 13d shows the mass fraction of methane at the exit of the vessel. The incline of the mass fraction over time occurs in the same order as found in Figures 13a-c. Both shrinking core models, although starting with the less steep slope, reach the limiting methane concentration in the shortest time.

3.3 Reduction of the Carrier Material NiO

As a third example of a possible carrier material NiO is considered which was incorporated in the CFD-study by

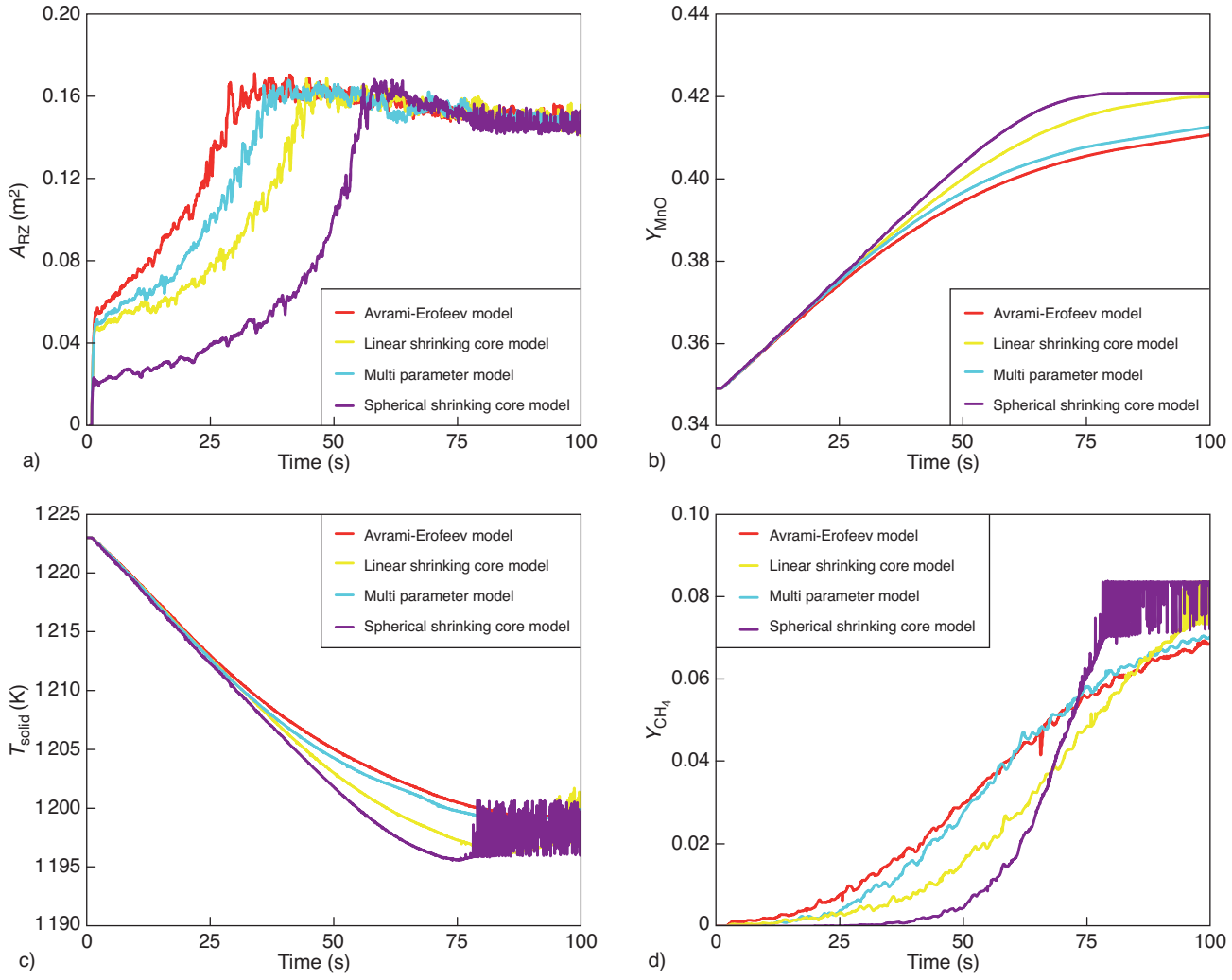

Figure 13

a) Area of the reaction zone, b) mass fraction of MnO in the solid phase, c) temperature of the solid phase and d) mass fraction of CH_4 at the outlet over time for $X_0 = 0.8$.

Jung and Gamwo [38], however, based on kinetics data by Ryu *et al*. [39] there. Here, kinetic data of Zafar *et al*. [53] is used. Figure 14 gives insight into the evolution of the conversion rate over the degree of conversion for NiO being exposed to methane. For both the experimental data obtained at constant temperature and at constant molar fraction of methane it gets obvious that NiO does not fully convert to Ni under the conditions considered by Zafar *et al*. [53]. A nucleation growth mechanism is not visible from the plots with conversion rates at zero conversion not being zero. Therefore, the application of the Avrami-Erofeev model seems not feasible. The linear shrinking core model reports a constant conversion rate which can not be confirmed for larger ranges of conversion. The spherical shrinking core model strongly underpredicts the experimentally derived conversion rates especially for low degrees of conversion. All three classical models have the disadvantage, that they assume a full conversion of NiO which is apparently not the case. In contrast, the empirically derived multi parameter model gives a far better representation of the experimental data. It is capable of modeling the incomplete conversion of NiO towards larger degrees of conversion. However, even for this model some deviations are detectable at low temperatures at constant methane concentration. The overall behavior, however, is still very good.

At low degrees of conversion the reaction rates reported from the Avrami-Erofeev model are very low. This is resulting in a very elongated reaction zone. The extension of the

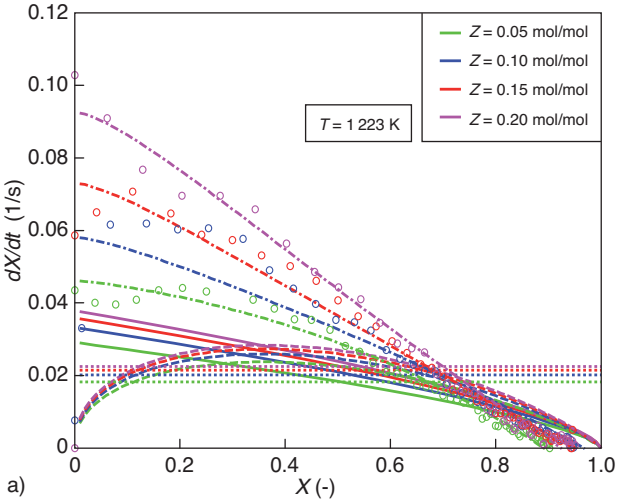

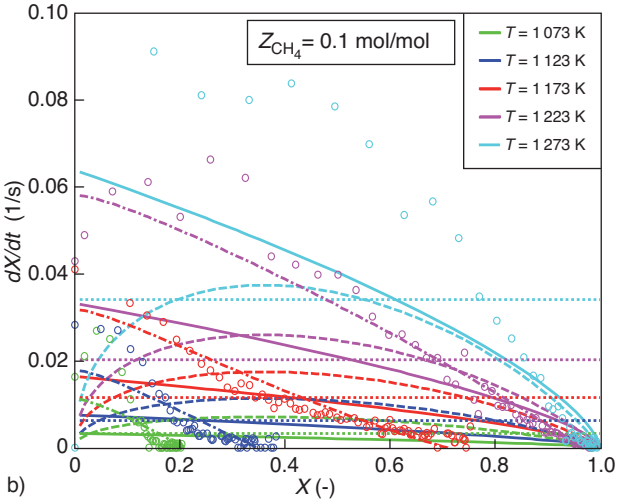

Figure 14

Conversion speed of NiO particles with CH_4 at the gas temperature T and molar fraction Z of the gaseous reactant: (—) spherical shrinking core model, (···) linear shrinking core model, (---) Avrami-Erofeev model, (-·-) multi parameter model, (○) experimental data derived by Zafar *et al.* [58].

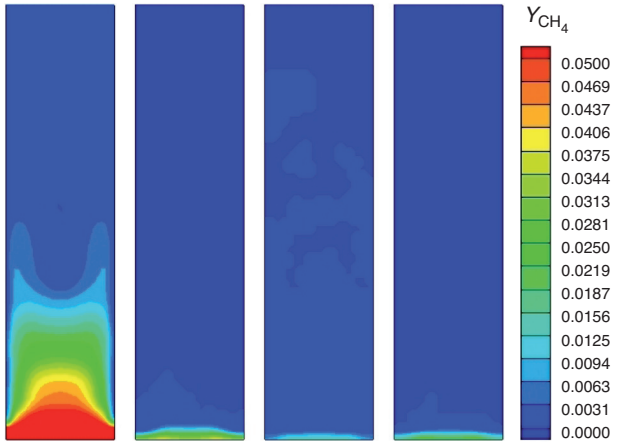

Figure 15

Mass fraction of CH_4 within the fluidized bed at t = 2 s. Reaction models from left to right: Avrami-Erofeev model, linear shrinking core model, multi parameter model and spherical shrinking core model.

reaction zone is, however, sufficient small enough to guarantee full conversion of the methane as displayed in Figure 15. All other three models result in significantly smaller reactions zones with the multi parameter model having the smallest zone. These results are in agreement with the observations from Figure 14.

Results for the initially fully unreacted NiO are outlined in Figure 16. With the Avrami-Erofeev model reporting an increasing reaction rate with progressing conversion, the size of the reaction zone defined as the area where $Y > 0.01$, is rapidly declining. At a certain progression a nearly equivalent large reaction zone is reported from all four models as shown in Figure 16a. With a full methane conversion being achieved within the vessel, the increase in Ni within the solid phase of the bed is the same for all four studied models *(Fig. 16b)*. Due to this and the fact that the reaction zones are of comparable size, an equal decreases in temperature for both the gas phase and the solid phase are reported over time.

At an elevated degree of conversion (X_0 = 0.8) studied in Figure 17 the overall reaction rate is reported so slow by the multi parameter model that the reaction zone expands over the whole dense phase region within the reaction vessel. At this point all other models still report a very fast reaction resulting in a small reaction zone as outlined in Figure 17a. The assumption of a fast reaction rate is made by the linear and the spherical shrinking core model over the whole range of considered simulation time. At t = 250 s the Avrami-Erofeev model reports a strong drop in reactivity resulting in an expansion of the reaction zone to the size reported by the multi parameter model. The methane concentration at the outlet is plotted in Figure 17b. Starting at X_0 = 0.8 no full conversion of methane is reported by the multi parameter model. The methane concentration is slowly increasing up to a point where the overall reaction stops and all injected methane is released unrendered from the vessel again. The same can be detected for the Avrami-Erofeev model where after t > 270 s all injected methane is released without reacting with the NiO. The halt of the reaction also gets visible from the plot of the gas outlet temperature in Figure 17c.

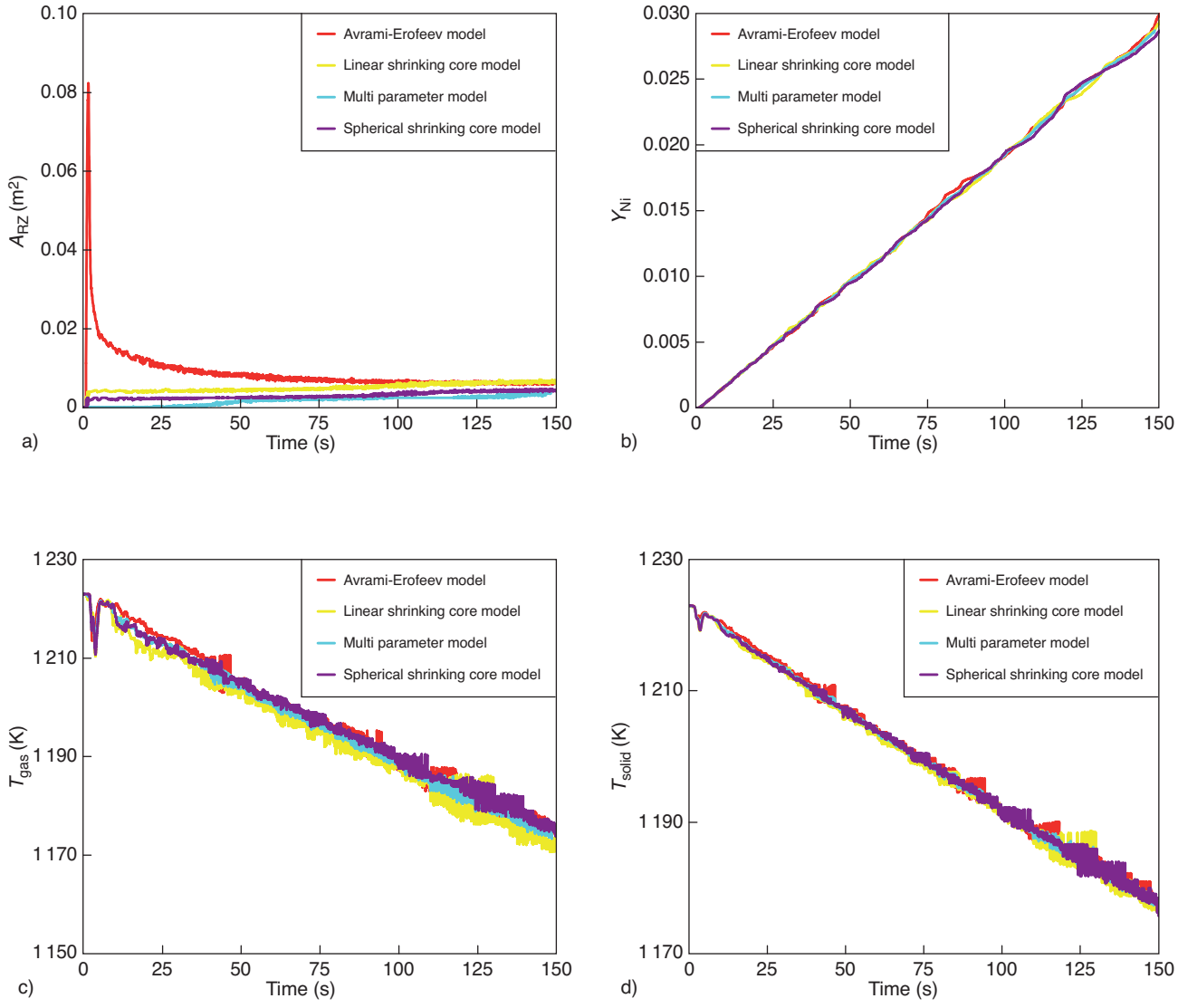

Figure 16

a) Area of the reaction zone, b) mass fraction of Ni in the solid phase, c) gas temperature at the outlet and d) temperature of the solid phase over time for $X_0 = 0$.

Whereas in the beginning the endothermic reaction results in a constant drop in the gas outlet temperature over time, the gas outlet temperature gets constant or slightly rising after the reaction comes to a halt. Taking a look at the Ni content in the solid phase in Figure 17d gives the impression that both the Avrami-Erofeev model and the multi parameter model leave the reaction halted abruptly. For the multi parameter model this is in clear agreement with the data on the kinetics shown in Figure 14. For the Avrami-Erofeev model the halt must be an effect of the strong decrease in reaction rate when approaching full degrees of conversion.

CONCLUSIONS

Due to the lack of investigations on the reaction modeling within fluidized systems used for chemical looping combustion three different oxygen carrier materials were investigated on a case by case basis. Four different kinetic models were considered whereas one was just proposed recently by Kruggel-Emden *et al*. [50]. For chemical looping combustion it is often assumed that gas/solid reactions of the carrier materials are sufficient fast [16], thereby leaving the kinetics and the selected kinetic model to have only minor

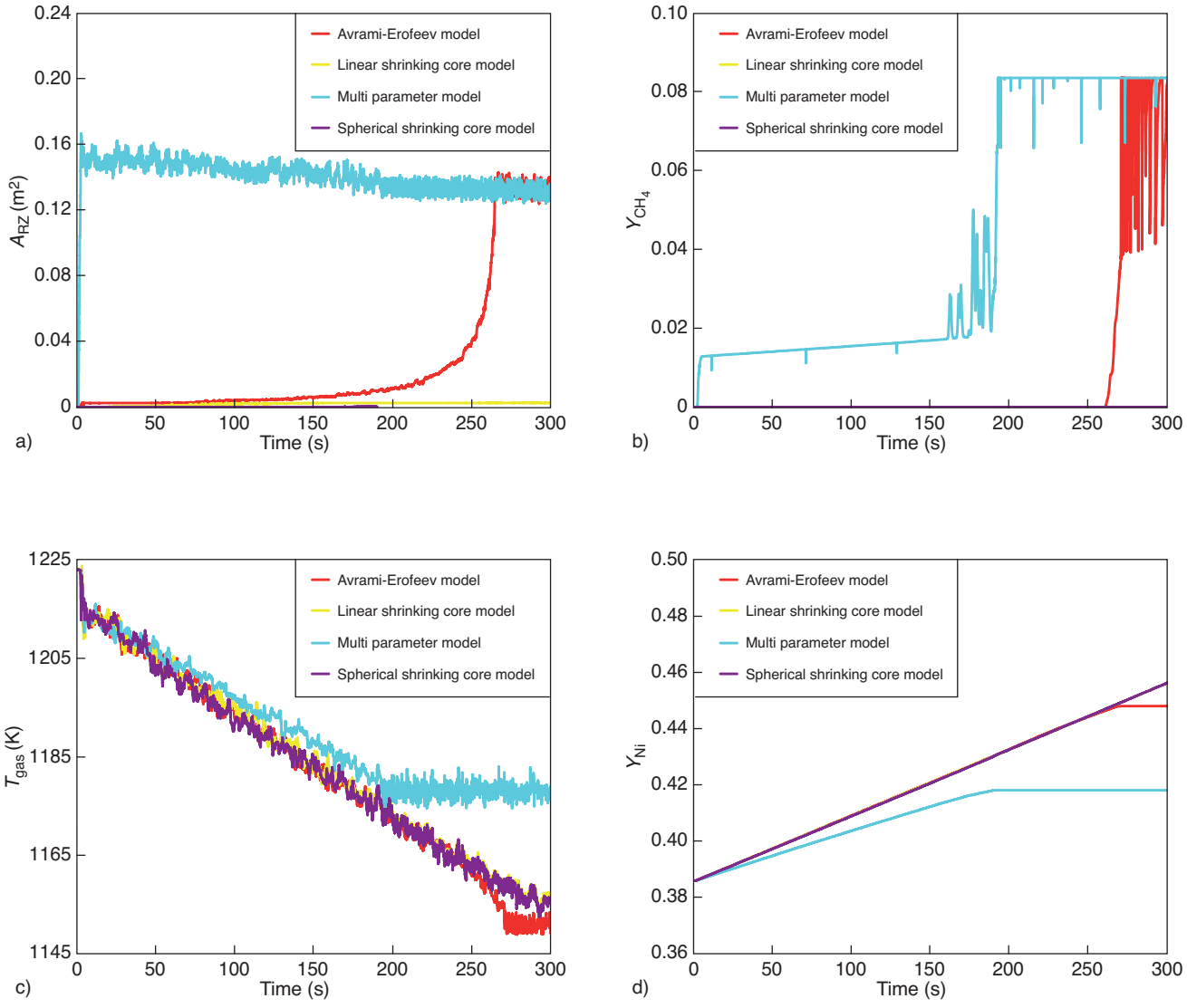

Figure 17

a) Area of the reaction zone, b) mass fraction of Ni in the solid phase, c) temperature of the gas mixture at the outlet and d) mass fraction of CH_4 at the outlet over time for $X_0 = 0.8$.

impact on macroscopic quantities within reaction vessels. This statement is true for some of the studied cases here and probably the majority of applications in which chemical looping combustion vessels are normally operated where it is desirable to achieve full conversion of the fuel or oxygen. However in simulations which consider scale-up of equipment, changes in design or transient modes of operation like start-up or other operational changes the conversion of the gaseous reactants may be temporarily incomplete. In these cases small changes in the kinetic models and the kinetic modeling data may have a strong impact on the quantities linked to a chemical looping reaction vessel. Therefore here sophisticated models have to be applied to guarantee for a correct modeling.

The study performed reveals the limitations associated with the classical models like the Avrami-Erofeev, the linear shrinking core and the spherical shrinking core model. They are not applicable over the whole range of conversion a carrier particle may encounter. A solution may pose multi parameter models [50] which are able to represent the correct limits of the conversion processes. Still the number of experiments providing data that could be used to adjust kinetic

models which could further be applied in multi phase CFD or particle oriented models is very limited. In particular, fuel gas mixtures lack detailed investigation. In general there is the strong need to perform more experimental investigations in order to get a better basis on which modeling can contribute to an enhancement of chemical looping combustion processes.

ACKNOWLEDGMENTS

The authors gratefully acknowledge the financial support by the Humboldt Foundation.

REFERENCES

1 IPCC Fourth Assessment Report, Paris, France (2007).

2 Herzog H., Eliasson B., Kaarstad O. (2000) Capturing greenhouse gases, *Sci. Am.* **282**, 2, 72-79.

3 Yang H., Xu Z., Fan M., Gupta R., Slimane R.B., Bland A.E., Wright I. (2008) Progress in carbon dioxide separation and capture: A review, *J. Environ. Sci.* **20**, 14-27.

4 Lyngfelt A., Lecker B. (1999) Technologies for CO_2 Separation, *Proceedings of the Minisymposium on CO_2 Capture and Storage*, Göteborg, Sweden.

5 Knoche K.F., Richter H. (1968) Verbesserung der Reversibilität von Verbrennungsprozessen, *Brennst.-Wärme-Kraft* **20**, 205-210.

6 Richter H.J., Knoche K.F. (1983) *Reversibility of combustion processes, Efficiency and Costing, Second Law Analysis of Processes*, Gaggioli R.A. (ed), *ACS Symp. Series* **235**, 71-85.

7 Lewis W.K., Gilliland E.R. (1954) *Production of pure carbon dioxide*, US Patent Nos. 2,665,971 and 2,665,972.

8 Ishida M., Zheng D., Akehata T. (1987) Evaluation of a Chemical-Looping-Combustion Power-Generation System by Graphic Exergy Analysis, *Energy* **12**, 2, 147-154.

9 Ishida M., Jin H.G. (1994) A New Advanced Power-Generation System Using Chemical-Looping Combustion, *Energy* **19**, 4, 415-422.

10 Hendriks C.A., Blok K., Turkenburg W.C. (1993) Promising Options to Remove Carbon Dioxide from Power Plants, *Proceedings of the International Symposium on CO_2 Fixation and Efficient Utilization of Energy*, Tokyo, Japan.

11 Naqvi R., Wolf J., Bolland O. (2007) Part-load analysis of a Chemical-Looping Combustion (CLC) combined cycle with CO_2 capture, *Energy* **32**, 360-370.

12 Lyngfelt A., Leckner B., Mattisson T. (2001) A fluidized-bed combustion process with inherent CO_2 separation; application of chemical-looping combustion, *Chem. Eng. Sci.* **56**, 10, 3101-3113.

13 Son S.R., Kim S.D. (2006) Chemical-Looping Combustion with NiO and Fe_2O_3 in a Thermobalance and Circulating Fluidized Bed Reactor with Double Loops, *Ind. Eng. Chem. Res.* **45**, 8, 2689-2696.

14 Gnanapragasam N.V., Reddy B.V., Rosen M.A. (2009) Hydrogen production from coal using coal direct chemical looping and syngas chemical looping combustion systems: Assessment of system operation and resource requirements, *Int. J. Hydrogen Energ.* **34**, 2606-2615.

15 Fan L., Li F., Ramkumar S. (2008) Utilization of chemical looping strategy in coal gasification processes, *Particuology* **6**, 131-142.

16 Noorman S., Annaland M.V., Kuipers H. (2007) Packed bed reactor technology for chemical-looping combustion, *Ind. Eng. Chem. Res.* **46**, 12, 4212-4220.

17 Noorman S., Annaland M.V., Kuipers J.A.M. (2009) Experimental validation of packed bed chemical-looping combustion, *Chem. Eng. Sci.* (in press).

18 Kim B.S., Sohn H.Y. (2002) A novel cyclic reaction system involving CaS and $CaSO_4$ for converting sulfur dioxide to elemental sulfur without generating secondary pollutants. 3. Kinetics of the hydrogen reduction of the calcium sulfate powder to calcium sulfide, *Ind. Eng. Chem. Res.* **41**, 13, 3092-3096.

19 Andrus H.E., Chiu J.H., Thibeault P.R., Brautsch A. (2009) Alstom's calcium oxide chemical looping combustion coal power technology development, *Proceedings of the 34th Internaional Technical Conference on Clean Coal & Fuel Systems*, Clearwater, Florida, USA.

20 Hossaina M.M., de Lasa H.I. (2008) Chemical-looping combustion (CLC) for inherent CO_2 separations - a review, *Chem. Eng. Sci.* **63**, 18, 4433-4451.

21 Abad A., Mattisson T., Lyngfelt A., Ryden M. (2006) Chemical-looping combustion in a 300 W continuously operating reactor system using a manganese-based oxygen carrier, *Fuel* **85**, 9, 1174-1185.

22 De Diego L.F., Garcia-Labiano F., Gayan P., Celaya J., Palacios J.M., Adanez J. (2007) Operation of a 10 kWth chemical-looping combustor during 200 h with a CuO-Al_2O_3 oxygen carrier, *Fuel* **86**, 7-8, 1036-1045.

23 Berquerand N., Lyngfelt A. (2008) The use of petroleum coke as fuel in a 10 kW(th) chemical-looping combustor, *Int. J. Greenhouse Gas Control* **2**, 2, 169-179.

24 Berguerand N., Lyngfelt A. (2008) Design and operation of a 10 kW(th) chemical-looping combustor for solid fuels - Testing with South African coal, *Fuel* **87**, 12, 2713-2726.

25 Adanez J., Dueso C., de Diego L.F., Garcia-Labiano F., Gayan P., Abad A. (2009) Methane Combustion in a 500 W-th Chemical-Looping Combustion System Using an Impregnated Ni-Based Oxygen Carrier, *Energ. Fuel.* **23**, 1, 130-142.

26 Kolbitsch P., Bolhar-Nordenkampf J., Proll T., Hofbauer H. (2009) Comparison of Two Ni-Based Oxygen Carriers for Chemical Looping Combustion of Natural Gas in 140 kW Continuous Looping Operation, *Ind. Eng. Chem. Res.* **48**, 11, 5542-5547.

27 Epple B., Stroehle J. (2008) CO_2 Capture based on carbonate and chemical looping, *VGB Powertech* **11**, 85-88.

28 Li F., Fan L.S. (2008) Coal conversion processes – progress and challenges, *Energ. Environ. Sci.* **1**, 248-267.

29 Simsek E., Brosch B., Wirtz S., Scherer V., Krüll F. (2009) Numerical Simulation of Grate Firing Systems using a Coupled CFD / Discrete Element Method (DEM), *Powder Technol.* **193**, 266-273.

30 Kruggel-Emden H., Stepanek F., Munjiza A. (2009) Discrete element methods for large scale particle/fluid simulations, *ASME Pressure Vessels & Piping Conference*, Prague, Czech Republic.

31 Ding J., Gidaspow D. (1990) A bubbling fluidization model using kinetic theory of granular flow, *AIChE J.* **32**, 1, 523-538.

32 Patil D.J., Annaland M.V., Kuipers J.A.M. (2004) Critical comparison of hydrodynamic models for gas–solid fluidized beds-part I: Bubbling gas–solid fluidized beds operated with a jet, *Chem. Eng. Sci.* **60**, 1, 57-72.

33 Patil D.J., Annaland M.V., Kuipers J.A.M. (2004) Critical comparison of hydrodynamic models for gas–solid fluidized beds-part II: Freely bubbling gas–solid fluidized beds, *Chem. Eng. Sci.* **60**, 1, 73-84.

34 Enwald H., Almstedt A.E. (1999) Fluid dynamics of a pressurized fluidized bed: Comparison between numerical solutions from two-fluid models and experimental results, *Chem. Eng. Sci.* **54**, 329-342.

35 Cooper S., Coronella C.J. (2005) CFD Simulation of particle mixing in a binary fluidized bed, *Powder Technol.* **151**, 27-36.

36 Vaishali S., Roy S., Mills P.L. (2008) Hydrodynamic simulation of gas–solids downflow reactors, *Chem. Eng. Sci.* **63**, 5107-5119.

37 Gryczka O., Heinrich S., Deen N.G., Annaland M.V., Kuipers J.A.M., Jacob M., Moerl L. (2009) Characterization and CFD-modeling of the hydrodynamics of a prismatic spouted bed apparatus, *Chem. Eng. Sci.* **64**, 3352-3375.

38 Jung J.W., Gamwo I.K. (2008) Multiphase CFD-based models for chemical looping combustion process: Fuel reactor modeling, *Powder Technol.* **183**, 3, 401-409.

39 Ryu H.J., Bae D.H., Han K.H., Lee S.Y., Jin G.T., Choi J.H. (2001) Oxidation and reduction characteristics of oxygen carrier particles and reaction kinetics by unreacted core model, *Korean J. Chem. Eng.* **18**, 831-837.

40 Levenspiel O. (1998) *Chemical Reaction Engineering*, New York, John Wiley and Sons.

41 Syamlal M., Rogers W., O'Brien T.J. (1993) *MFIX documentation theory guide*, Technical Note, DOE/METC-94/1004, NTIS/DE94000087, U.S. Department of Energy, Office of Fossil Energy, Morgantown Energy Technology Center Morgantown, WV, National Technical Information Service, Springfield, VA.

42 Deng Z.Y., Xiao R., Jin B.S., Song Q.L., Huang H. (2008) Multiphase CFD Modeling for a Chemical Looping Combustion Process (Fuel Reactor), *Chem. Eng. Technol.* **31**, 12, 1754-1766.

43 Deng Z.Y., Xiao R., Jin B.S., Song Q.L. (2009) Numerical simulation of chemical looping combustion process with $CaSO_4$ oxygen carrier, *Int. J. Greenhouse Gas Control* **3**, 4, 368-375.

44 Jin B.S., Xiao R., Deng Z.Y., Song Q.L. (2009) Computational Fluid Dynamics Modeling of Chemical Looping Combustion Process with Calcium Sulphate Oxygen Carrier, *Int. J. Chem. Reactor Eng.* **7**, A19.

45 Xu M., Ellis N., Ryu H.J., Lim C.J. (2007) Modeling of an Interconnected Fluidized Bed Reactor for Chemical Looping Combustion, *The 12th International Conference on Fluidization*, Vancouver, Canada.

46 Bolhar-Nordenkampf J., Proll T., Kolbitsch P., Hofbauer H. (2009) Comprehensive Modeling Tool for Chemical Looping Based Processes, *Chem. Eng. Technol.* **32**, 3, 410-417.

47 Kolbitsch P., Proll T., Hofbauer H. (2009) Modeling of a 120 kW chemical looping combustion reactor system using a Ni-based oxygen carrier, *Chem. Eng. Sci.* **64**, 1, 99-108.

48 Kruggel-Emden H., Rickelt S., Stepanek F., Munjiza A. (2010) Development and testing of an interconnected multiphase CFD-model for chemical looping combustion, *Chem. Eng. Sci.* **65**, 16, 4732-4745.

49 Gidaspow D. (1994) *Multiphase Flow and Fluidization*, Academic Press, San Diego.

50 Kruggel-Emden H., Stepanek F., Munjiza A. (2009) A comparative study of reaction models for chemical looping combustion, *Comput. Chem. Eng.* (submitted).

51 Zafar Q., Abad A., Mattisson T., Gevert B., Strand M. (2007) Reduction and oxidation kinetics of Mn_3O_4/Mg-ZrO_2 oxygen carrier particles for chemical-looping combustion, *Chem. Eng. Sci.* **62**, 6556-6567.

52 Johansson M., Mattisson T., Lyngfelt A. (2006) Investigation of Mn_3O_4 with stabilized ZrO_2 for chemical-looping combustion, *Chem. Eng. Res. Des.* **84**, A9, 807-818.

53 Zafar Q., Abad A., Mattisson T., Gevert B. (2007) Reaction kinetics of freeze-granulated NiO/$MgAl_2O_4$ oxygen carrier particles for chemical-looping combustion, *Energ. Fuel.* **21**, 2, 610-618.

Final manuscript received in October 2010
Published online in February 2011